ORIGINAL PAPER

Effect of GMAW Process Parameters and Heat Input on Weld Overlay of Austenitic Stainless Steel 316L-Si

Joyce Ingrid Venceslau de Souto[1] , Suzana Dantas Ferreira[1] , Jefferson Segundo de Lima[1,2] , Walman Benicio de Castro[1] , Estephanie Nobre Dantas Grassi[1] , Tiago Felipe de Abreu Santos[2]

[1] Universidade Federal de Campina Grande – UFCG, Departamento de Engenharia Mecânica, Campina Grande, PB, Brasil.
[2] Universidade Federal de Pernambuco – UFPE, Departamento de Engenharia Mecânica, Recife, PE, Brasil.

Abstract: Overlay welding with stainless steels has gained attention in several sectors of industry by increasing the mechanical and electrochemical properties of surfaces, in order to obtain them using lower cost substrates. However, the control of welding parameters can become complex due to the multiple control variables, being of interest to obtain deposits with greater productivity. In this context, the objective of this paper is to analyze the effect of the heat input on weld overlays of austenitic stainless steel 316L-Si obtained by the GMAW process, to determine the best welding conditions. For this, a Design of Experiments was implemented to analyze the response variables, which include heat input, reinforcement, width, dilution and hardness of the weld metal. The models were considered significant, presenting $R^2>0.9$ for all responses, based on a 95% confidence limit. Surface graphs indicated influence of welding speed or/and voltage for all responses, in addition to the results demonstrating optimal parameters for overlays such as high ratio between reinforcement and width (0.631), and low dilution values (8.81%). The microstructural analysis indicated the presence of residual γ-austenite and δ-ferrite in all samples, and also the formation of peninsulas and islands, added to defects such as voids, for some weld deposits.

Key-words: GMAW process; Heat input; Stainless steel 316LSi; DoE.

1. Introduction

Several welding processes, or their variations, are used for the deposition of material on a surface, aiming at the recovery of worn parts or for the formation of a coating with special characteristics [1]. The combination of carbon steel adopted as substrate for the coated stainless steel is suitable for various applications that require high mechanical strength combined with good corrosion resistance, especially in the petroleum, petrochemical, shipbuilding and pressure vessel industries [2].

The broad field of applications for overlays obtained by welding, using mainly stainless steel alloys as filler metal, has been promoting the growth of studies related to the influence of heat input on the microstructure and the optimization of mechanical properties in coated products [3]. High alloy stainless steels, such as 316L, with higher chromium, molybdenum and nickel contents, are one of the most studied in the series, as they are characterized by high corrosion resistance, good ductility, high strength and good weldability at relatively low costs [4]. 316LSi stainless steel is a special grade of austenitic stainless steels (ASS) with the addition of molybdenum, which increases an indicator of high resistance to pitting corrosion, and the addition of silicon, which stabilizes ferrite in the austenite matrix in a level that provides greater resistance to solidification cracks [5].

Among the main overlay welding processes employed in the industry, as described by AWS (2004), the *Gas Metal Arc Welding* (GMAW) process is a popular and effective method, which can be semi-automated, easy to operate and with high productivity [6]. The performance of this process can be improved with the adoption of appropriate process parameters depending on the alloys and variables used [7]. Fusion welding requires heat to melt the contact surface (substrate) and the filler material (filler metal) so that coalescence can be effected and a welded joint with good mechanical and metallurgical characteristics is obtained after solidification. Thus, the heat input plays a significant role in welding, especially in the characteristics of the weld bead geometry, and can be quantified as a function of the welding current, welding voltage and torch displacement speed, depending on the foreseen metallic transfer mode [7,8].

It is known that coating processes, especially those involving heat input such as welding, require that their products have specified characteristics for validation of the procedure, such as low dilution and penetration values, in addition to optimal ratios of reinforcement and deposit width. In this context, it is extremely important to understand how the multiple input variables of the process influence the characteristics of the deposits, through experimental techniques [9,10], ANOVA [7,11], and neural network application [12,13]. In this context, prospective studies on the analysis of the effect of heat input and selection of welding parameters to obtain weld overlays in austenitic stainless steel 316L-Si by the GMAW process are of great relevance for the understanding and optimization of the physical and metallurgical properties in coatings for industrial application, as well as the growth of the technical bibliography specialized in welding.

2. Methodology

2.1. Model for design of experiments

The experiments were based on two factors, directly related to heat input, with two levels through first-order full factorial design. The independent input variables of the input process were welding speed (200 to 300 mm·min^{-1}) and electric arc voltage (22 to 26 V). The range of values for both factors was selected based on the literature concerning the GMAW process with the same class of deposited material [14-17]. The experimental data are analyzed by the response surface methodology using the software Statistica. The F-test and analysis of variance (ANOVA) serve to evaluate the adequacy of the developed mathematical models. The experimental data were fitted with the first order polynomial equation by the regression method to identify related terms in the mathematical model [18] in Equation 1

$$y(x_1, x_2) = \beta_0 + \beta_1 x_1 + \beta_2 x_2 + \beta_{12} x_{12} + \varepsilon(x_1, x_2) \tag{1}$$

where β_0 is the average value of all factorial design responses; β_1, β_2 e β_{12} are the population values of the two main effects and the interaction effect for each x_1 e x_2; and $\varepsilon(x_1, x_2)$ is the random error associated with the response $y(x_1, x_2)$.

2.2. Experimental execution

In this work, an AISI 1015 steel was used as substrate and a stainless steel ER316L-Si wire of a diameter 1.2 mm was used as weld overlay. Both nominal chemical compositions are presented in Tables 1 and 2. The dimensions of each substrate to be overlayed were 100 mm long x 50 mm wide by 6.35 mm thickness. All welds were performed in the horizontal position and without preheating.

Table 1. Nominal chemical composition (weight %) of the AISI 1015 steel.

%C	%Mn	%Cr	%Zn	%Fe
0.148	0.419	0.043	0.033	balance

Table 2. Nominal chemical composition (weight %) of filler metal ER316L-Si.

%C	%Cr	%Ni	%Mo	%Mn	%Si	%P	%S	%Cu
0.03	18.0-20.0	11.0-14.0	2.0-3.0	1.0-2.5	0.65-1.0	0.03	0.03	0.75

During all depositions, commercial argon gas (99.8% Ar) was used as a shielding gas, maintaining it at a flow rate of 16 L·min^{-1}. The contact tip-to-work distance (CTTW) was maintained at 20 mm and the wire at a rate of 6 m·min^{-1} continuously fed the torch. The variation of the parameters in the different depositions was carried out according to the range of values observed in Table 3, based on specialized literature [19-21].

Table 3. Input parameters and experimental limits.

Parameters	Level -1	Level 0	Level +1
Welding speed, WS (mm·min^{-1})	200.0	250.0	300.0
Welding voltage, WV (V)	22.0	24.0	26.0

All samples were transversely sectioned in the middle region of the weld beads, embedded, sanded to 2400 grain size, polished in silica solution and chemically etched with acidic glycerin (3 parts HCl + 2 parts glycerol + 1 part nitric acid). For the metallographic analysis, an optical microscopy (Olympus, SC30) was used. For the macrograph analysis of the weld deposit, a stereoscopic equipment (Kontrol, KET-300) was used with a 10x magnification, and post-processing of the images was carried out in the software Image J in order to estimate the areas of reinforcement of the weld metal and penetration into the base metal of each welded bead for the calculation of dilution.

The voltage and the welding speed are independent variables when calculating the heat input of the welding, being estimated from Equation 2:

$$H_l = \frac{60*WV*WC}{WS} * \eta \tag{2}$$

where H$_l$ corresponds to the heat input, in kJ·m^{-1}; WV corresponds to the welding voltage, in V; WC corresponds to the welding current, in A; WS corresponds to the welding speed, in mm·min^{-1}; and η corresponds to the efficiency of the welding process,

taken as 0.75 for the GMAW process [1, 22]. Concomitantly with the execution of the welds, the data referring to the welding signals were stored by means of a data acquisition system (IMC Soldagem, SAT) with a rate of 5000 Hz, from which the effective average value of WC and WV were extracted to estimate H_I for each sample.

For the Vickers hardness test, carried out in a digital microdurometer (Future-Tech, FM-700), a load of 500 g was used for an indentation time of 15 s. In each specimen, the hardness measurements were made in the region of the weld metal, in a 4 x 2 matrix pattern of indentations spaced 0.5 mm apart. The output parameters measured by the macrograph, as well as the diagrammatic scheme of the indentations made during the hardness test, are shown in Figure 1.
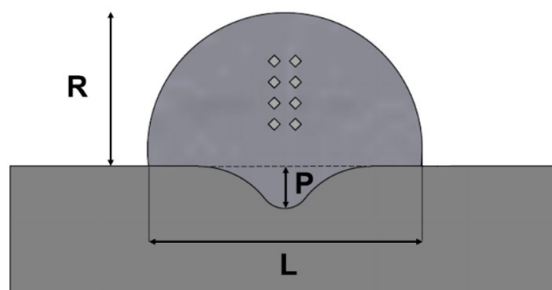

Figure 1. Schematic diagram of output geometric parameters, where "R" indicates height, "L" indicates width, and "P" indicates penetration, for the overlay welds.

As shown in Figure 1, the height (R), width (L) and penetration (P) of the welds were determined, together with a form factor ($R \cdot L^{-1}$), dilution (D) of the weld metal in relation to the substrate, and the average value of the indentations hardness (H). The mentioned output parameters were used to evaluate the relationship among these and the process parameters, as well as the heat input through regression models and analysis of the response surfaces.

3. Results and discussions

Figure 2 shows the cross sections of the welded samples for different welding parameters levels (welding speed and voltage variation). After preliminary visual inspection, very distinct conditions are verified in the geometric aspects of the deposited weld beads. Especially, it was possible to observe notable differences for the responses of penetration, dilution and width of the deposits, which were properly evaluated by the post-processing of the macrographs, whose evaluated output parameters were categorically measured.
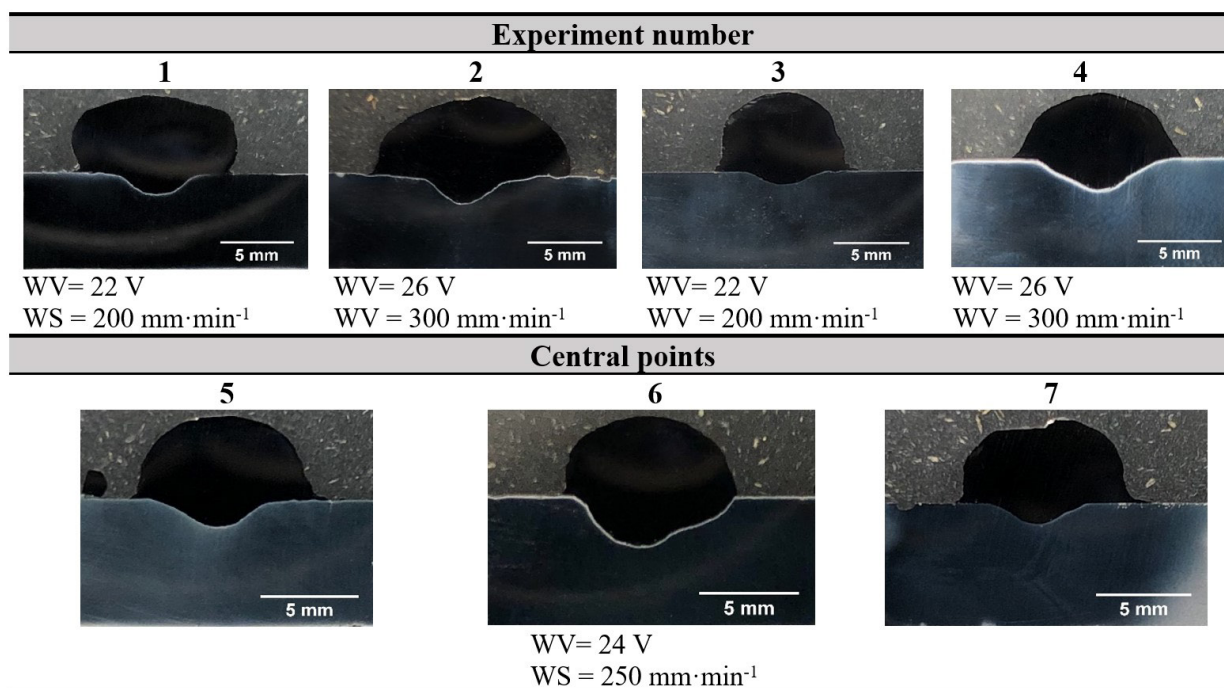

Figure 2. Macrograph of the embedded welded samples.

The experiments were conducted with a view to the specified factorial design and the samples were cross-sectioned for the analysis of the responses mentioned in Table 4.

Table 4. Matrix of factorial design $2^2 + 3$ for the overlay welds.

Exp. No.	WC (A)	WV (V)	H_l (kJ·m^{-1})	R (mm)	L (mm)	R·L^{-1}	D (%)	H (HV)
1	161.860	22.461	817.996	5.148	10.370	0.496	14.85	175.988
2	169.395	26.244	1000.263	5.251	13.197	0.398	18.19	174.525
3	171.549	22.348	575.061	4.874	7.723	0.631	8.81	178.388
4	184.936	26.222	727.400	3.751	9.739	0.385	28.66	187.125
5	174.736	24.349	765.840	4.600	10.200	0.451	18.64	180.025
6	180.988	24.251	790.050	4.750	10.000	0.475	19.00	180.500
7	169.300	24.257	739.214	4.690	9.316	0.503	15.00	179.000

3.1. ANOVA – Analysis of Variance

Analysis of variance helped to test the adequacy of the models. For this test, the calculated F-value must be within the confidence limit (95%) for $p < 0.05$ [7], since statistical models with a reliability of 95% have high reliability and predictive capacity. The fit values indicate that the mathematical models are significant for all output responses. The final reduced models for the output responses are derived from Tables 5 to 8 of the ANOVA results, presenting the formats described by Equations 3 to 6. P values less than 0.05 are highlighted in bold.

Table 5. ANOVA results for heat input H_l.

Factors	Sum of squares	Degrees of freedom	Mean square	F-value	P-value
WS	66511.8900	1	66511.8900	118.3230	**0.0017**
WV	27990.2211	1	27990.2211	49.7939	**0.0058**
WS·WV	223.9365	1	223.93650	0.3984	0.5727
Error	1686.3637	3	562.1212	-	-
Sum squared total	96412.4113	6	-	-	-

$R^2 = 98.251$; $R^2_{adjusted} = 96.502$.

$$H_l = 773.689 - 128.949 \cdot WS + 83.651 \cdot WV \tag{3}$$

Table 6. ANOVA results for the **R·L^{-1}** ratio.

Factors	Sum of squares	Degrees of freedom	Mean square	F-value	P-value
WS	0.0037	1	0.0037	8.0718	0.0656
WV	0.0297	1	0.0297	64.4326	**0.0040**
WS·WV	0.0054	1	0.0054	11.7982	**0.0414**
Error	0.0014	3	0.0005	-	-
Sum squared total	0.0402	6	-	-	-

$R^2 = 96.564$; $R^2_{adjusted} = 93.127$.

$$\frac{R}{L} = 0.47714 - 0.08612 \cdot WV - 0.03685 \cdot WS \cdot WV \tag{4}$$

Table 7. ANOVA results for dilution D.

Factors	Sum of squares	Degrees of freedom	Mean square	F-value	P-value
WS	4.9062	1	4.9062	3.7222	0.1493
WV	134.4440	1	134.4440	101.9992	**0.0021**
WS·WV	68.1450	1	68.1450	51.6999	**0.0055**
Error	3.9543	3	1.3181	-	-
Sum squared total	211.4495	6	-	-	-

$R^2 = 98.130$; $R^2_{adjusted} = 96.260$.

$$D = 17.8071 + 5.7975 \cdot WV + 4.1275 \cdot WS \cdot WV \tag{5}$$

Table 8. ANOVA results for hardness H.

Factors	Sum of squares	Degrees of freedom	Mean square	F-value	P-value
WS	56.2500	1	56.2500	71.1684	**0.0035**
WV	13.2278	1	13.2278	16.7360	**0.0264**
WS*WV	26.0100	1	26.0100	32.9083	**0.0105**
Error	2.3711	3	0.7904	-	-
Sum squared total	97.8589	6	-	-	-

R^2 = 97.577; $R^2_{adjusted}$ = 95.1540

$$H = 179.3644 + 3.7500 \cdot WS + 1.8185 \cdot WV + 2.5500 \cdot WS \cdot WV \qquad (6)$$

The adjustment of the models was expressed by the coefficient of determination ($R^2_{adjusted}$), which was higher than 90% for all ANOVAs. Since an R^2 value approaching 100% indicates a better fit between the model and observed responses, the $R^2 > 90\%$ suggests that the calculated models can satisfactorily predict the experimental responses [18]. However, to confirm whether the proposed model is statistically significant and predictive, an analysis of variance (ANOVA) was also performed.

The data presented in Tables 5 to 8 demonstrate that the statistical models of all output variables are significant and predictive, for effects with $p < 0.05$, according to the values of R^2 e $R^2_{adjusted}$ observed in the ANOVA.

3.2. Influence of process parameters on heat input

The heat input (H_I) can, in this case, be treated as a response variable, given that one of the independent variables for its calculation – the welding current (WC) – is treated as a response variable. This is justified by the selected transfer mode (conventional) and its respective control parameters. In this, the welding current is equivalent to the amperage output of the source during the deposition of the beads, being related to the wire feed speed and environmental conditions [23].

As previously observed by the ANOVA table, and depending on the control parameters, there are results of high statistical significance for the heat input which validate the consolidated mathematical relationships used to calculate the input. Moreover, it is possible to establish that there was no noticeable influence of statistical randomness or experimental instability for this response variable. The response surface graphs for the influence of the speed and voltage welding parameters on the heat input obtained from the ANOVA are presented in Figure 3.
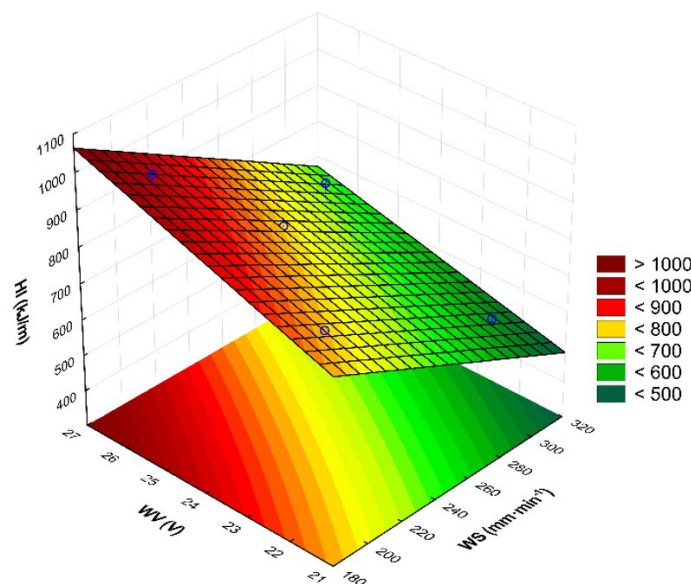

Figure 3. Heat input response surface graph in deposited weld beads.

By analyzing the response graph in Figure 3, it can be seen that lower values of heat input are the result of low values of welding voltage combined with high values of welding speed [11, 14, 21]. Normally, high heat input values are not reflected in good results in overlay applications because it culminates in a high level of residual tensile stresses and distortion, which compromises the physical and mechanical integrity of the coated products [24]. On the other hand, very low heat input values

can cause defects such as lack of penetration, or lack of fusion and voids [1]. In this sense, a selection of parameters based on adequate H_l values observed in the response surface can be taken as a viable solution for the prevention of welding defects.

3.3. Influence of process parameters on geometric characteristics

The response surface graphs for the geometric characteristics of the depositions, obtained from the results of the ANOVA table, can be seen in Figure 4. The variables of width/reinforcement and dilution, respectively, were analyzed as a function of the variation of the WS and WV.
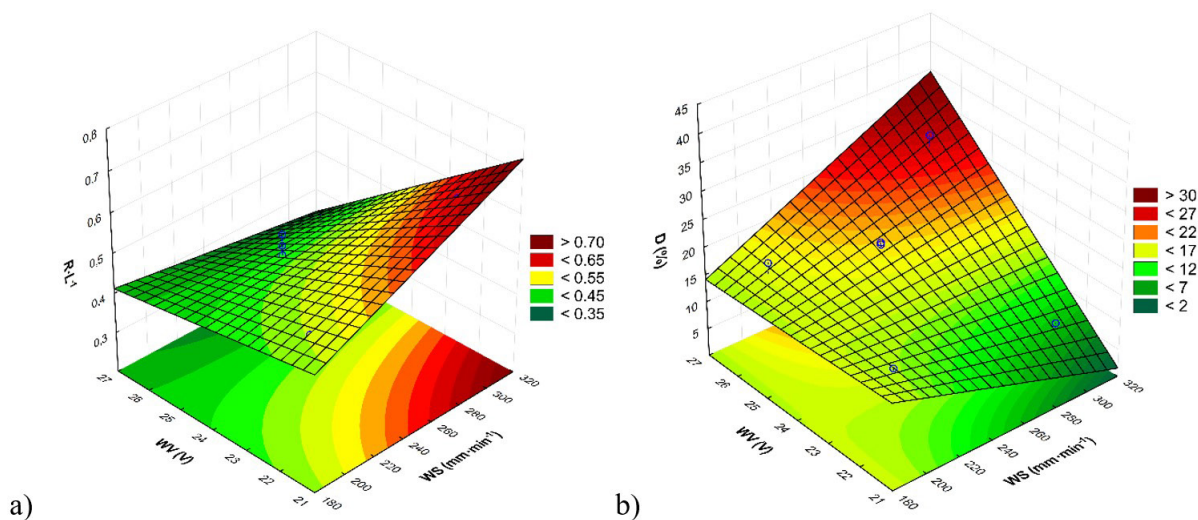

Figure 4. Response surface plots of a) width/reinforcement ratio, and b) dilution on deposited weld beads.

With regard to reinforcement (R), Figure 4a, this response increases significantly when the welding speed is increased and welding voltage decreased [25], which suggests that higher heat input values tend to result in weld beads with higher reinforcement values [21] for depositing stainless steel 316LSi. A similar analysis refers to Figure 4a, demonstrating that the reduction in the welding speed together with the increase in voltage causes a considerable increase in the width of the bead [25], which can be inferred that higher values of heat input tend to result in greater bead widths [21] for stainless steel 316LSi.

Both reinforcement and bead width can be analyzed together with the $R \cdot L^{-1}$ ratio, termed as the inverse of the reinforcement form factor (RFF). In this perspective, the analysis of Figure 3a presents an inverse relationship with the heat input, so that it is possible to obtain weld deposits with higher $R \cdot L^{-1}$ values, which reflects in an overlay with less spreading on the substrate with lower values of heat input within the range of values calculated in the present study [7, 21, 26]. Considering that a good overlay weld is one that manages to cover the largest possible area of the substrate [25], the best conditions for the $R \cdot L^{-1}$ ratio are those that obtain its maximum value (the closest to 1), which are the employed in sample 3 (22 V and 200 mm·min^{-1}).

In parallel analysis, for dilution, the response surface in Figure 4b indicates that low percentages of dilution are obtained when simultaneously employing low voltage values with high welding speeds [25, 27]. With regard to the effectiveness of overlay welds, dilution values greater than 20% are not recommended for a satisfactory overlay in terms of preserving the characteristics of the weld metal [20]. In general, low levels of dilution were obtained, as shown in Table 4, with the exception of sample 4 (D = 28.66%), which was justified by the highest WC level identified among the samples (WC = 184.936 A) [28].

In a similar analysis, sample 3 showed the lowest dilution of the factorial design (D = 8.81%), based mainly on the lowest heat input value among the samples (H_l = 575.061 kJ·m^{-1}) [29], being a result of good relevance for further work on parameter optimization for overlay welding using the GMAW process with stainless steel 316L-Si. Thus, the lowest dilution presented among the samples configures the best condition of the welding parameters, in the range of values analyzed, which was presented by sample 3, when combining the welding speed at 200 mm·min^{-1} and the welding voltage at 22 V.

3.4. Influence of process parameters on hardness

Analogously to what was presented in the previous section, the response surface for the hardness as a function of the welding speed and voltage, presented in Figure 5, was significant based on the ANOVA results, to the detriment of the adopted reliability.
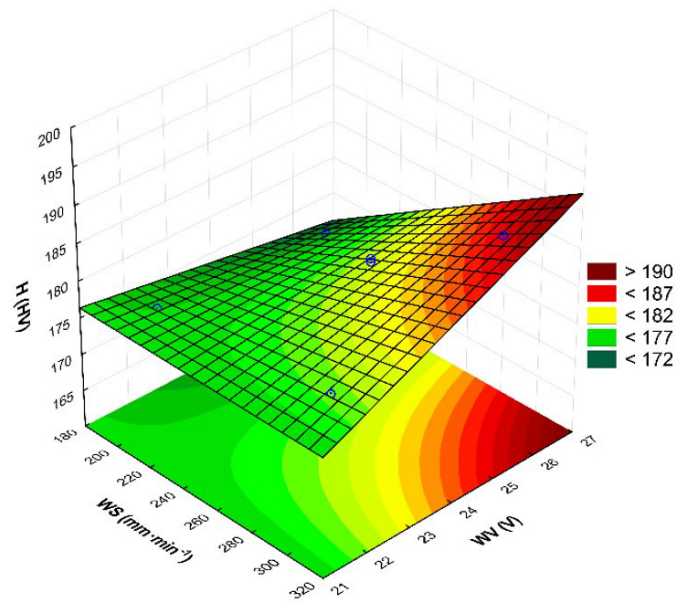
Figure 5. Hardness response surface graph in deposited weld beads.

In terms of absolute values, the experiments demonstrated hardness values within the range of 174.525 HV and 187.125 HV for austenitic stainless steel 316L-Si, [30] when applying a heat input of 520 kJ·m^{-1} [29]. The response surface graph observed in Figure 5 suggests that higher hardness values are obtained by combining high values of welding speed and voltage. As both factors are concurrently related to heat input, both value ranges can be used to investigate how hardness will be influenced by input. There was an increase in hardness measured between 500 and 800 kJ·m^{-1} [19, 31]. It has already been described in the literature that, for lower values of heat input, in a comparative way, there is a tendency to obtain a greater number of indentations with high hardness values (Table 4) [32], which was also observed in the present work.

3.5. Microstructural analysis

In the metallographic analysis, the weld deposit was observed according to the microstructural state of the Heat Affected Zone (HAZ). From this, the microstructures obtained from samples 2 and 4 are observed in Figures 6 and 7, with heat inputs equivalent to 1000.263 kJ·m^{-1} and 727.400 kJ·m^{-1}, respectively.
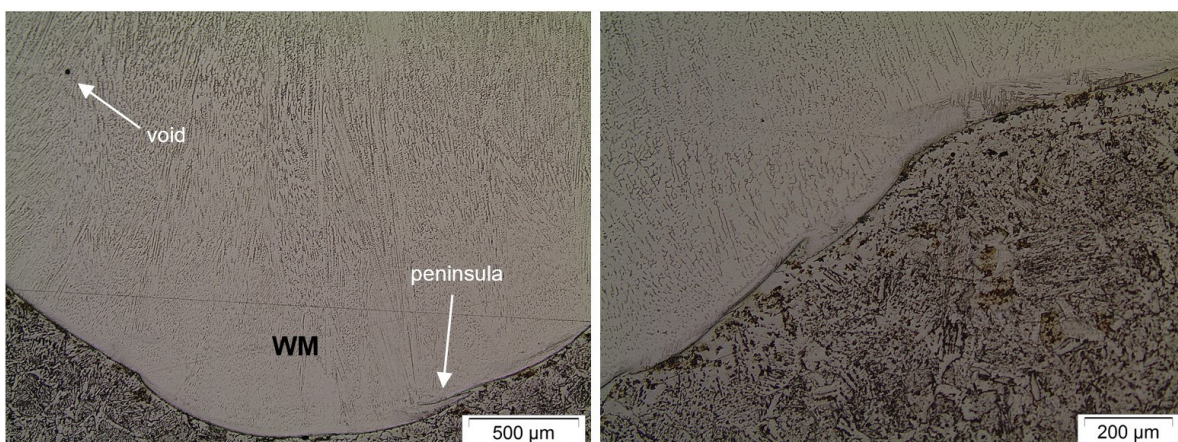

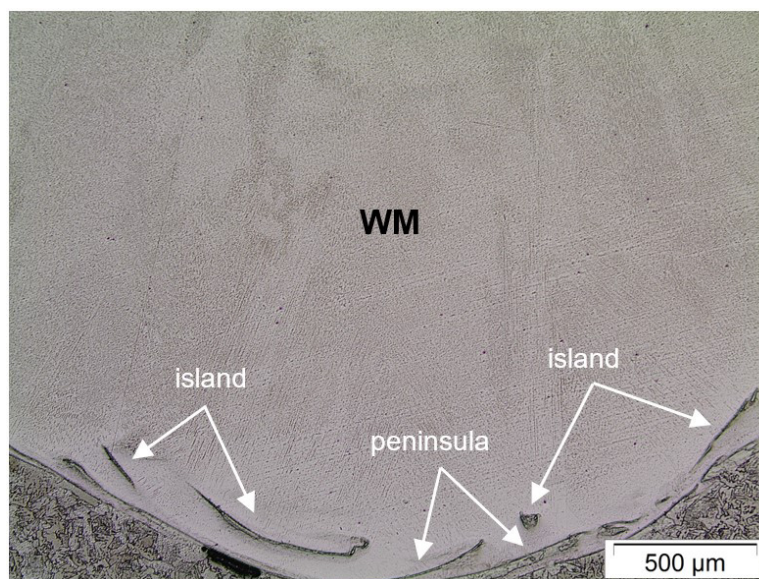**Figure 6.** Micrograph of sample 2. Etch: acidic glycerin.

Figure 7. Micrograph of sample 4. Etch: acidic glycerin.

In general, the weld metal microstructure of all samples showed pearlite (dark region) and ferrite (light region) in the refined grains. It is also possible to observe the presence of columnar dendrites of γ-austenite (in white) and some residues of δ-ferrite (in black) in the region of the deposit, observed in Figure 6 on the right, predicted for deposition of austenitic stainless steel with addition of silicon [33], and when the deposition was performed using stainless steel 316LSi [5]. The residual δ-ferrite was mainly distributed in the austenite boundaries for the weld overlay of the same class of material with the addition of molybdenum and 316LSi [34, 35]. On the other hand, the base metal microstructure in the HAZ region for all samples, as exemplified on the right in Figure 6, is composed of bainite and pearlite [36,37].

It is observed that sample 4, Figure 7, presented differentiated morphologies called "peninsula" and "islands" swirl patterns, at the interface between the WM (Weld Metal) and the BM (Base Metal) [38,39]. These grains are part of the so-called Partially Diluted Zone (PDZ) which is characterized by the penetration of WM into the BM [40,41]. Such morphologies were also presented in previous studies [32, 39, 42]. The regions observed in Figures 6 and 7 are also present for samples 6 (H_l=790.050 kJ·m^{-1}) and 7 (H_l=739.214 kJ·m^{-1}).

The greater amount of unmelted particles may be related to whether the intensity of current used is sufficient or not to ensure complete fusion of the WM [20]. For the welding conditions that produced samples 1, 4 and 5, they did not present any type of defect in their microstructure. In samples 2 and 3, the presence of voids was observed in the deposit region, close or not to the melting line, which can be explained by the low average level of WC [20].

4. Conclusions

Through the factorial experimental design, mathematical response models were obtained for the variables related to the macrograph characterization, with the geometric parameters of reinforcement (R), width (L), and dilution (D), in addition to the mechanical characterization, with the response of hardness (H). All mathematical models proved to be statistically significant and predictive, resulting in values for coefficient of determination above 90% for all analyzed response variables. The presented results confirm the use of DoE as a useful tool for optimization and selection of welding parameters.

With regard to the geometric characteristics, the welding voltage parameter was the most significant for the R·L^{-1} form factor and dilution, in view of its direct influence on the weld deposit spreading and heat input, which collaborates in the degree of penetration of the weld metal to the substrate. Lower welding voltage levels generated better results for the dilution (14.85% for sample 1, and 8.81% for sample 3), when using 22 V, and for the R·L^{-1} ratio, whose best results were obtained for its highest values (0.631 for sample 3 and 0.503 for sample 7), when using 22 V and 24 V, respectively. For the geometric characteristics, the best results of the response factors observed and analyzed via DoE, indicating the best combination of input parameters, were obtained in sample 3 obtained by combining a welding speed of 200 mm·min^{-1} and a welding voltage of 22 V.

For hardness, all factors, as well as their interaction, were significant for the results, demonstrating a subtle increase with the increase in heat input, in view of its relationship with the cooling rate of the deposit, which influences the formation of harder constituents. It is noteworthy that high levels of welding speed produced better hardness results (187.125 HV for sample 4), when using 300 mm·min^{-1}, while using higher levels of welding speed together with higher levels of welding voltage produced comparable hardness results (180.025 HV for sample 5, 180.5 HV for sample 6, and 179.0 HV for sample 7), when using 250 mm/min and 24 V. Therefore, for the output parameters of heat input and Vickers hardness (HV), it was considered that the

best results were obtained by samples whose applied parameters were at their average level. Thus, the best conditions for these responses were shown by setting the welding speed at 250 mm·min^{-1} and the welding voltage at 24 V.

For the microstructural analysis, the microconstituents foreseen in the deposit region, namely residual γ-austenite and δ-ferrite, were in accordance with the type of filler material employed. Furthermore, some discontinuities inherent to the welding process, such as voids, were observed in the weld beads. In this case, the use of low levels of welding current was attributed to the appearance of this type of defect in some samples (169.395 A for sample 2, and 171.549 A for sample 3), relating them to incomplete melting of the weld metal.

Authors' contributions

JIVS: conceptualization, data curation, formal analysis, investigation, methodology, validation, writing – original draft, writing – review & editing. **SDF**: conceptualization, data curation, investigation, methodology, visualization, writing – original draft. **JSL**: formal analysis, methodology, supervision, validation, writing – review & editing. **WBC**: supervision, validation, writing – review & editing. **ENDG**: conceptualization, methodology, supervision, validation, writing – review & editing. **TFAS**: supervision, writing – review & editing.

Acknowledgements

References

[1] Modenesi PJ, Marques PV, Belo DBS. Introdução à metalurgia da soldagem. 1st ed. Belo Horizonte: UFMG; 2012.

[2] Di Schino A, Testani C. Corrosion behavior and mechanical properties of AISI 316 stainless steel clad Q235 plate. Metals. 2020;10(4):1-14. http://dx.doi.org/10.3390/met10040552.

[3] Silva MM, Oliveira WC, Maciel TM, Santos MA, Motta MF. caracterização de solda de revestimento de AWS 317L depositados por GMAW duplo arame em aços ASTM A 516 Gr 60 para uso na indústria do petróleo. Rev Eletrônica Mater e Process. 2019;15:225-233.

[4] Belsvik MA, Tucho WM, Hansen V. Microstructural studies of direct-laser-deposited stainless steel 316L-Si on 316L base material. SN Appl Sci. 2020;2(12):1967. http://dx.doi.org/10.1007/s42452-020-03530-3.

[5] Raut LP, Taiwade RV, Agarwal A. Investigation of microstructural and corrosion behavior of 316LSi structure developed by wire arc additive manufacturing. Materials Today. Communications. 2023;35:105596. http://dx.doi.org/10.1016/j.mtcomm.2023.105596.

[6] Welding Handbook AWS. Welding processes: part 1. Danvers: American Welding Society; 2004. Vol. 2.

[7] Saha MK, Hazra R, Mondal A, Das S. Effect of heat input on geometry of austenitic stainless steel weld bead on low carbon steel. J Inst Eng Ser C. 2019;100(4):607-615. http://dx.doi.org/10.1007/s40032-018-0461-7.

[8] Madavi KR, Jogi BF, Lohar GS. Investigational study and microstructural comparison of MIG welding process for with and without activated flux. Materials Today: Proceedings. 2022;51:212-216. http://dx.doi.org/10.1016/j.matpr.2021.05.240.

[9] Lázaro-Lobato LÁ, Curiel-López FF, López-Morelos VH, García-Rentería MA. Taguchi methodology approach on microstructural and mechanical properties of bimetallic welded joints of API 5L X-52/AISI 316L-Si. MRS Advances. 2023;8(2):27-33. http://dx.doi.org/10.1557/s43580-022-00479-w.

[10] Kumar V, Ranjan Sahu D, Mandal A. Parametric study and optimization of GMAW based AM process for Multi-layer bead deposition. Materials Today: Proceedings. 2022;62:255-261. http://dx.doi.org/10.1016/j.matpr.2022.03.223.

[11] Krishna Kumar G, Velmurugan C, Jayaram RS, Manikandan M. Effect of laser welding process parameters on dissimilar joints of AISI 316 and nickel 201. Materials Today: Proceedings. 2020;22:2964-2973. http://dx.doi.org/10.1016/j.matpr.2020.03.431.

[12] Wang Y, Xu X, Zhao Z, Deng W, Han J, Bai L, et al. Coordinated monitoring and control method of deposited layer width and reinforcement in WAAM process. Journal of Manufacturing Processes. 2021;71:306-316. http://dx.doi.org/10.1016/j.jmapro.2021.09.033.

[13] Xiao X, Waddell C, Hamilton C, Xiao H. Quality prediction and control in wire arc additive manufacturing via novel machine learning framework. Micromachines. 2022;13(1):137. http://dx.doi.org/10.3390/mi13010137. PMid:35056302.

[14] Sen M, Mukherjee M, Singh SK, Pal TK. Effect of double-pulsed gas metal arc welding (DP-GMAW) process variables on microstructural constituents and hardness of low carbon steel weld deposits. Journal of Manufacturing Processes. 2018;31:424-439. http://dx.doi.org/10.1016/j.jmapro.2017.12.003.

[15] Abioye TE, Ariwoola OE, Ogedengbe TI, Farayibi PK, Gbadeyan OO. Effects of welding speed on the microstructure and corrosion behavior of dissimilar gas metal arc weld joints of AISI 304 stainless steel and low carbon steel. Materials Today: Proceedings. 2019;17:871-877. http://dx.doi.org/10.1016/j.matpr.2019.06.383.

[16] Nasir NSM, Abdul MKAR, Ahmad MI, Mamat S. Influence of heat input on carbon steel microstructure. ARPN J Eng Appl Sci. 2017;12:2689-2697.

[17] Biswas AR, Chakraborty S, Ghosh PS, Bose D. Study of parametric effects on mechanical properties of stainless steel (AISI 304) and medium carbon steel (45C8) welded joint using GMAW. Materials Today: Proceedings. 2018;5(5):12384-12393. http://dx.doi.org/10.1016/j.matpr.2018.02.217.

[18] Barros B No, Scarminio IS, Bruns RE. Como fazer experimentos: pesquisa e desenvolvimento na ciência e na indústria. Campinas: UNICAMP; 2001.

[19] Gomes NL, Henrique F, Saboia C, Ferreira H, Abreu G. Efeito da variação da corrente elétrica de soldagem na microestrutura e na microdureza de ligas Fe-Cr-Mo com diferentes teores de Mo. Rev Conexões. 2011;5(3):36-47.

[20] Nunes EB, Cavalcante NE, Barreto AS, Silva AÍN, Motta MF. Avaliação do efeito da energia de soldagem na deposição de aço inoxidável superduplex pelo processo plasma pó. Soldagem e Inspeção. 2015;20(2):205-218. http://dx.doi.org/10.1590/0104-9224/SI2002.08.

[21] Biyikli M, Karagoz T, Calli M, Muslim T, Ozalp AA, Bayram A. Single track geometry prediction of laser metal deposited 316L-Si via multi-physics modelling and regression analysis with experimental validation. Metals and Materials International. 2023;29(3):807-820. http://dx.doi.org/10.1007/s12540-022-01243-3.

[22] Kou S. Welding metallurgy. 2nd ed. New Jersey: John Wiley & Sons; 2003. Vol. 4. https://doi.org/10.22486/iwj.v4i3.150243.

[23] Naidu DS, Ozcelik S, Moore KL. Gas metal arc welding: automatic control. In: Naidu DS, Ozcelik S, editors. Moore sensing and control of gas metal arc welding KLBT-M. Oxford: Elsevier Science Ltd; 2003. p. 147-218. http://dx.doi.org/10.1016/B978-008044066-8/50006-9.

[24] Tomar B, Shiva S, Nath T. A review on wire arc additive manufacturing: processing parameters, defects, quality improvement and recent advances. Materials Today. Communications. 2022;31:103739. http://dx.doi.org/10.1016/j.mtcomm.2022.103739.

[25] Gomes JHF, Costa SC, Paiva AP, Balestrassi PP. Otimização de múltiplos objetivos na soldagem de revestimento de chapas de Aço carbono ABNT 1020 utilizando arame tubular inoxidável austenítico. Soldagem e Inspeção. 2011;16(3):232-242. http://dx.doi.org/10.1590/S0104-92242011000300005.

[26] Ramasamy S, Sivasubramanian R, Yoganandh J. Effect of automated MIG welding process parameters on ASTM A 106 Grade B pipe weldments used in high-temperature applications. Materials and Manufacturing Processes. 2017;33:1-10. http://dx.doi.org/10.1080/10426914.2017.1401719.

[27] Silva ASC, Araújo HR, Macena VA, Moreno JRS, Vicente AA, Hermenegildo TF, et al. Aplicação da metodologia para qualificação de procedimentos de soldagem de tubulações industriais conforme parâmetros dos códigos ASME B31.3 e ASME SECTION IX*. Soldagem e Inspeção. 2019;24:e2423. http://dx.doi.org/10.1590/0104-9224/si24.23.

[28] Jindal S, Chhibber R, Mehta N. Effect of welding parameters on bead profile, microhardness and H 2 content in submerged arc welding of high-strength low-alloy steel. Proceedings of the Institution of Mechanical Engineers. Part B, Journal of Engineering Manufacture. 2014;228(1):82-94. http://dx.doi.org/10.1177/0954405413495846.

[29] Varghese P, Vetrivendan E, Dash MK, Ningshen S, Kamaraj M, Kamachi Mudali U. Weld overlay coating of Inconel 617 M on type 316 L stainless steel by cold metal transfer process. Surface and Coatings Technology. 2019;357:1004-1013. http://dx.doi.org/10.1016/j.surfcoat.2018.10.073.

[30] Guimarães RF. Efeito da energia de soldagem na zona afetada pelo calor do aço inoxidável ferrítico AISI 444. Rev Conex. 2010;4:41-47.

[31] Muthusamy C, Karuppiah L, Paulraj S, Kandasami D, Kandhasamy R. Effect of heat input on mechanical and metallurgical properties of gas tungsten arc welded lean super martensitic stainless steel. Materials Research. 2016;19(3):572-579. http://dx.doi.org/10.1590/1980-5373-MR-2015-0538.

[32] Silva MM, Maciel TM, dos Santos MA, Motta MF. Lima M do SSS. Efeito da energia de soldagem sobre a microestrutura de revestimentos AISI 317L depositados em aços ASTM A516 Gr 60 para aplicação no setor de petróleo e gás. Rev Eletrônica Mater e Process. 2010;2:54-60.

[33] Chen C, Feng T, Sun G, Zhang H. Microstructure and mechanical characteristics of 307Si stainless steel thin-wall parts in wire arc additive manufacturing hybrid interlayer high-speed friction. Manufacturing Letters. 2022;33:42-45. http://dx.doi.org/10.1016/j.mfglet.2022.07.009.

[34] Cunha HM. Caracterização de juntas soldadas de aços carbono e aços inoxidáveis utilizando arame AWS E309L T1-1 [masters dissertation]. Ilha Solteira: UNESP; 2016.

[35] Veiga F, Arizmendi M, Suarez A, Bilbao J, Uralde V. Different path strategies for directed energy deposition of crossing intersections from stainless steel SS316L-Si. Journal of Manufacturing Processes. 2022;84:953-964. http://dx.doi.org/10.1016/j.jmapro.2022.10.039.

[36] Silva CC, Assis JT, Philippov S, Farias JP. Residual stress, microstructure and hardness of thin-walled low-carbon steel pipes welded manually. Materials Research. 2016;19(6):1215-1225. http://dx.doi.org/10.1590/1980-5373-mr-2016-0217.

[37] Rajakumar S, Vimal Kumar P, Kavitha S, Balasubramanian V. Mechanical and microstructural characteristics of conventional and robotic gas metal arc welded low carbon steel joints: a comparative study. Metallogr Microstruct Anal. 2020;9(3):337-344. http://dx.doi.org/10.1007/s13632-020-00645-2.

[38] Yang YK, Kou S. Weld-bottom macrosegregation caused by dissimilar filler metals. Welding Journal. 2007;86:373-379.

[39] Dodge MF, Dong HB, Gittos MF, Mobberley T. Fusion zone microstructure associated with embrittlement of subsea dissimilar joints. In: Proceedings of International Conference on Offshore Mechanics and Artic Engineering. New York: ASME; 2014. http://dx.doi.org/10.1115/OMAE2014-23643.

[40] Silva MM. Caracterização metalúrgica e tenacidade de revestimentos em aços inoxidáveis 317L aplicados por soldagens MIG manual e robotizado para equipamentos do setor de petróleo e gás [masters dissertation]. Campina Grande: Universidade Federal de Campina Grande; 2009.

[41] Batista V, Pereira E, Fraga R, Maciel T. Efeito do tratamento térmico de alívio de tensão e do preaquecimento na microestrutura e microdureza da interface entre depósitos de inconel 625 e aços AISI 8630M e AISI 4130. Matéria (Rio de Janeiro). 2021;26(1):e12920. http://dx.doi.org/10.1590/s1517-707620210001.1220.

[42] Dai T, Lippold JC. The effect of postweld heat treatment on hydrogen-assisted cracking of 8630/alloy 625 overlay. Welding in the World. 2018;62(3):581-599. http://dx.doi.org/10.1007/s40194-018-0578-6.